

LASER BIOPHOTONICS

PACS numbers: 87.50.U–; 87.19.L–
DOI: 10.1070/QE2014v044n08ABEH015486

Numerical and experimental studies of mechanisms underlying the effect of pulsed broadband terahertz radiation on nerve cells

M.V. Duka, L.N. Dvoretskaya, N.S. Balbekin,
M.K. Khodzitskii, S.A. Chivilikhin, O.A. Smolyanskaya

Abstract. **We have studied the mechanisms underlying the effect of pulsed broadband terahertz radiation on the growth of neurites of sensory ganglia using a comparative analysis of measured reflection spectra of ganglion neurites (in the frequency range 0.1–2.0 THz) and spectra obtained by numerical simulation with CST Microwave Studio. The observed changes are shown to be mainly due to pulse energy absorption in the ganglion neurites. Of particular interest are the observed single resonance frequencies related to resonance size effects, which can be used to irradiate ganglia in order to activate their growth.**

Keywords: *terahertz radiation, influence mechanisms, ganglia, neurites.*

1. Introduction

Recent years have seen increased interest in the study of the effect of terahertz (THz) radiation on biological objects. The reason for this is that the THz range includes the frequencies of low-energy rovibrational levels of an enormous number of bioactive molecules with a complex spatial structure (such as proteins, RNA and DNA) and their functional groups, as well as the frequencies of collective vibrational transitions at the intermolecular level, responsible for intermolecular interactions [1]. Intensive research effort has been concentrated on methods for assigning lines in the THz spectra of biomolecules: analysis of the hybridisation state of DNA [2] and investigation of vibrations and rotations of particular atomic groups [3], sensitivity to protein conformations and their mutations [4] and the eigenfrequencies of DNA [5]. Unfortunately, at the present stage in the development of spectroscopy the above methods are incapable of assigning each spectral line of complex biomolecules because of their extremely complex structure and the large number of intermolecular bonds. The spectroscopy of cells and tissues is even less capable of providing unambiguous information because these consist of a large number of organelles (nuclei, mitochondria, cytoplasm and others), which are in turn composed of a diversity of biological molecules.

M.V. Duka, L.N. Dvoretskaya, N.S. Balbekin, M.K. Khodzitskii, S.A. Chivilikhin, O.A. Smolyanskaya St. Petersburg State University of Information Technologies, Mechanics and Optics, Kronverkskii prosp. 49, 197101 St. Petersburg, Russia; e-mail: duka.mv@yandex.ru, khodzitskiy@yandex.ru, o_smolyanskaya@mail.ru

Received 3 March 2014; revision received 16 June 2014
Kvantovaya Elektronika **44** (8) 707–712 (2014)
Translated by O.M. Tsarev

The ability to identify the origin of spectral lines of biological objects will provide greater insight into the mechanisms underlying the effect of THz radiation, which are still only tentatively understood. The strong absorption of high-power THz radiation by hydrated biological tissues may cause thermal effects [6]. In addition to bulk thermal effects, microthermal effects are possible, which result from direct sequential excitation of biomolecules [7] or from linear/nonlinear resonance mechanisms [8, 9], and an ultrasonic wave may be generated [10]. These effects may cause the following response of a cell: changes in the conformation of membrane proteins and in the cell membrane permeability to various substances, electric charge redistribution on the cell membrane and excitation of resonance vibrations in the macromolecules present in the cell membrane and cytoskeleton.

Experimental studies concerned with the effect of THz radiation on biological objects differ significantly in radiation characteristics and objects. Use is made of both continuous-wave (cw) and pulsed radiation sources differing in characteristics: wavelength, output power, pulse duration, pulse repetition rate and exposure time. The results obtained to date differ widely, which prevents them from being structured and makes it impossible to ascertain whether THz radiation has an advantageous or adverse effect and, especially, to identify the underlying mechanisms. In the case of cw sources, there is the highest probability to elucidate the mechanism, because a biomarker can be found more readily: precisely what is influenced by radiation at a particular frequency. With pulsed broadband sources, an effect may be due to a combined influence of radiation at several frequencies on various cell components. One possible consequence is the multiplicativity of irradiation at different frequencies, which leads to ambiguities in data interpretation even within one experiment. For example, irradiation in the range 2–20 THz may increase the expression of some genes and reduce that of others [11]. To understand the origin of this effect and to achieve a more effective influence of radiation at a particular wavelength, it is necessary to carry out a support study using a variety of frequency filters transmitting a particular frequency range of pulsed THz radiation. To detect the effect, it can be investigated further using cw radiation sources at a particular frequency. To this end, an immense number of search studies at various frequencies are needed.

The high water content of biological objects may play a key role in determining the effect of radiation on cells, because water has many absorption lines in the THz frequency range. Therefore, these lines will be present as well in the spectrum of a biological object. Moreover, spectral features of an object may be due as well to resonance size effects over the optical length of its macrostructure (Fabry–Perot resonances).

Eliminating the frequencies related to absorption lines of water and the resonance frequencies related to the generation of standing waves in the structure allows one to identify spectral lines unrelated to the intermolecular interactions of hydrated cell components.

To eliminate the last two factors, it is necessary to model the propagation of broadband pulses through a hydrated biological object with geometric dimensions corresponding to those of an object used in an experiment and to carry out a comparative analysis of measured spectra of biological objects and water and the spectra obtained by numerical simulation.

In this paper, we present a comparative analysis of measured and simulated reflection spectra of a sample of spinal ganglia in the frequency range 0.1–2.0 THz with the aim of elucidating the mechanism underlying the effect of pulsed broadband THz radiation on the growth of neurites of sensory ganglia.

2. Sample preparation

The chick embryo spinal ganglion (organotypic nerve tissue culture) is one of the most convenient experimental models for investigation because it responds to any physical and chemical stimuli by enhancing or suppressing the growth of sensitive extensions (neurites). A ganglion, or a nerve knot, is a cluster of nerve, glial and Schwann cells, whose sizes are about 20, 7 and 6–8 μm, respectively. Adults have two types of nerve cells, with cell diameters of 20–30 and 20–50 μm [12].

Spinal ganglia were removed and prepared using an eye surgery kit. The ganglia were removed from ten-day chick embryos at the level of the lumbosacral spine under a microscope and were placed in a polystyrene Petri dish with a collagen substrate. To assess the effect of THz radiation on neurite growth, controls and irradiated samples were cultured in an incubator (5% carbon dioxide) for three days at a temperature of 36.8 °C. Before measurements of reflection spectra, the Petri dishes were placed in the incubator for 30 min to ensure better fixation of the explants to the substrate.

3. Effect of THz radiation on neurite growth

Spinal ganglion samples 0.1 cm^2 in area, enclosed in a Petri dish, were exposed to pulsed broadband THz radiation (frequency range 0.1–2.0 THz; pulse duration, 2.5 ps) for 3 and 5 min at a temperature of +25 °C [13]. We carried out a comparative analysis of ten control samples and ten samples irradiated at various incident THz powers (0.076–11.600 μW). The incident power was varied using filters, with allowance for the absorption of the radiation by the Petri dish.

Neurite growth in tissue culture was studied *in vivo* for three days after irradiation and culturing, using a Carl Zeiss LSM 710 optical microscope equipped with a Carl Zeiss Axiostar Plus accessory. The effect of THz radiation was assessed morphometrically, from the area index: the ratio of the area of the entire cultured sample, including the peripheral growth zone, to the initial ganglion area (Fig. 1). The area index of the controls was taken to be 100%.

As the incident power was decreased, we observed first a depressive and then a stimulating effect of THz radiation on neurite growth. The growth stimulation effect reached 147 ± 22% (significance level $p < 0.05$) relative to the controls at a THz power density of about 1.1 μW cm^{-2}.

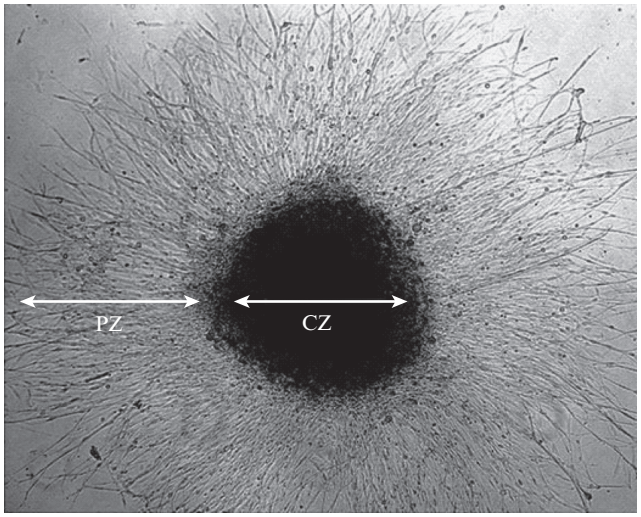

Figure 1. Micrograph of a control sample of a ten-day chick embryo spinal ganglion (magnification of 50×). CZ and PZ are the central and peripheral zones of the ganglion, respectively.

4. Technique for measuring THz reflection spectra of ganglia

Reflection spectra were obtained using a pulsed THz reflectometer (Fig. 2). Pulsed broadband THz radiation (spectral range 0.1–2.0 THz; average power, 30 μW; pulse peak power,

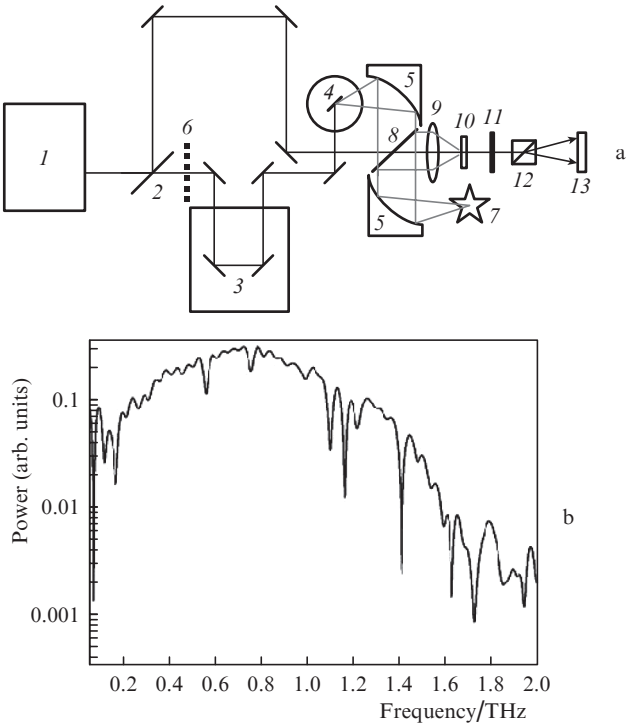

Figure 2. (a) Schematic of the THz reflectometer and (b) frequency spectrum of a THz pulse: (*1*) femtosecond laser, (*2*) beam splitter, (*3*) optical delay line, (*4*) THz generator (InAs crystal in a magnetic system), (*5*) 45° parabolic mirrors, (*6*) optomechanical chopper, (*7*) biological object under study, (*8*) THz beam splitter from a high-resistivity silicon plate, (*9*) TPX lens with a 5-cm focal length, (*10*) CdTe electro-optical crystal, (*11*) achromatic quarter-wave plate, (*12*) Wollaston prism, (*13*) balanced photodetector.

755 μW; pulse duration, 2.7 ps) was generated by a photoconductive antenna (undoped indium arsenide crystal), which was exposed to femtosecond Yb:KYW laser pulses (wavelength, 1040 nm; pulse duration, 120 fs; pulse repetition rate, 75 MHz; output power, 1 W). Most of the THz power was concentrated in the frequency range 0.12–1.10 THz [13].

After passing through a Teflon filter (which eliminated wavelengths under 50 μm), the terahertz radiation generated by an InAs crystal in a magnetic system propagated through a sample (ganglia enclosed in a Petri dish) fixed in a vertical position in the focal plane, normal to the beam, on a three-coordinate stage. The beam first passed through the substrate and then impinged on the ganglia. When a femtosecond probe beam and the THz beam reflected from the sample combined on a CdTe electro-optical crystal, the terahertz pulse induced birefringence of the probe beam in the crystal owing to the electro-optical effect. The birefringence value was proportional to the electric field amplitude $E(t)$ of the THz wave at a given point in time. The birefringence measurement system comprised a quarter-wave plate, Wollaston prism, balanced photodetector (Nirvana) and lock-in amplifier (Femto LIA-MV-150), controlled by an optomechanical chopper (Thorlabs MC-1000A) placed in the path of the pump beam.

In the absence of THz radiation, the probe beam experienced no birefringence. After passing through the quarter-wave plate, which transformed horizontal beam polarisation into circular one, and through the Wollaston prism, the probe beam was divided into two components identical in intensity, with orthogonal polarisations. As a consequence, there was no signal at the output of the balanced photodetector. When a THz pulse induced birefringence in the electro-optical crystal, the beams differed in intensity after passing through the Wollaston prism, and the balanced photodetector produced a mismatch signal (Fig. 2). A delay line was used to vary the point in time when the THz and probe pulses coincided in the nonlinear crystal. In this way, by measuring the THz signal as a function of time delay, we obtained a time-dependent THz field amplitude $E(t)$. To increase the signal-to-noise ratio, a lock-in amplifier was used. The filtered and amplified signal was fed to a computer through an ADC. The setup ensured a spectral resolution of 15 GHz. The spectrometer was automated by means of a virtual instrument created in the LabView environment, which allowed us to record the temporal profile of the THz pulse, $E(t)$, and calculate the reflection spectrum of the sample. Spectra were obtained by Fourier transforming the temporal profile of the measured (reference and test) pulses and calculating the ratio of the amplitude of the spectrum of the reference signal to that of the biological object.

5. Simulation with CST Microwave Studio

To model the THz response of biological objects, we used CST Microwave Studio – software for 3D electromagnetic simulation of structures of arbitrary shape. Biological objects were simulated as hydrated structures because of the increased percentage of water (78%) in nerve cells. The real and imaginary parts of the dielectric permittivity of water that were used in our simulations are presented in Fig. 3 [14, 15].

We considered two bilayer structures, one comprising a substrate and a layer of a hydrated biological object (Fig. 4a), and the other, a substrate and a biological object consisting of hydrated spherical particles (Fig. 4b). The ganglion was modelled as an accumulation of nerve cell phantoms, which made a major contribution to the spectral characteristics of the biological object owing to their large size. Glial and Schwann cells were left out of consideration. The nerve cells were represented as randomly arranged spherical resonators 17–22 μm in diameter. The cell conglomerate had a 800-μm thickness and was situated on a 950-μm-thick polystyrene substrate (permittivity $\varepsilon = 4.326$) [16]. The structure was excited in free space by a plane electromagnetic wave in the frequency range 0.1–2.0 THz. Since the membrane thickness (0.01 μm) and nucleus diameter (1 μm) differ greatly from THz wavelengths, the various organelles of the nerve cells were left out of consideration in our simulations. The biological object was located between two ports: emitter (port 1) and receiver (port 2). Simulation of the former structure was necessary to identify the spectral resonance lines due to the generation of standing waves over the optical thickness of the structure, and the latter structure was investigated in order to detect resonance size effects of the nerve cells.

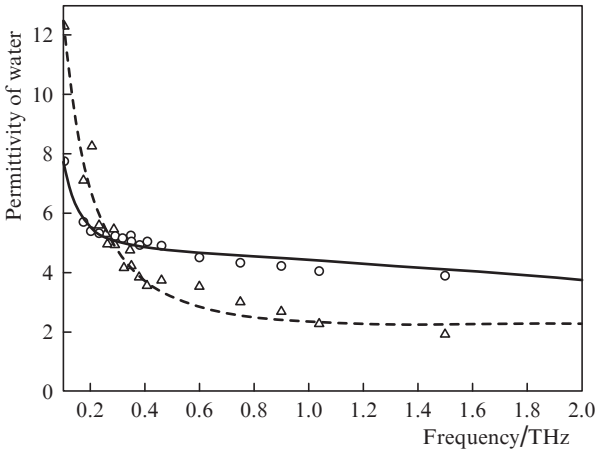

Figure 3. Real (○) and imaginary (△) parts of the relative dielectric permittivity of water. The curves represent theoretical fits to the data.

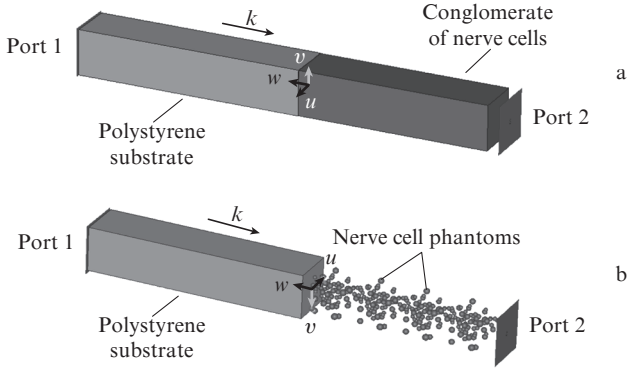

Figure 4. CST Microwave Studio models of the system under study: (a) substrate and a layer of a hydrated biological object, (b) substrate and a biological object consisting of hydrated spherical particles. Port 1: THz emitter; port 2: receiver.

To examine the effect of nerve cell size on the reflection spectrum, we simulated structures with three cell diameter (D) distributions, having D in the ranges 20–30, 20–40 and 20–50 μm. The distributions were taken to be normal, with a probability density

$$f(D) = \frac{1}{\sigma\sqrt{2\pi}} \exp\left[-\frac{(D-\bar{D})^2}{2\sigma^2}\right],$$

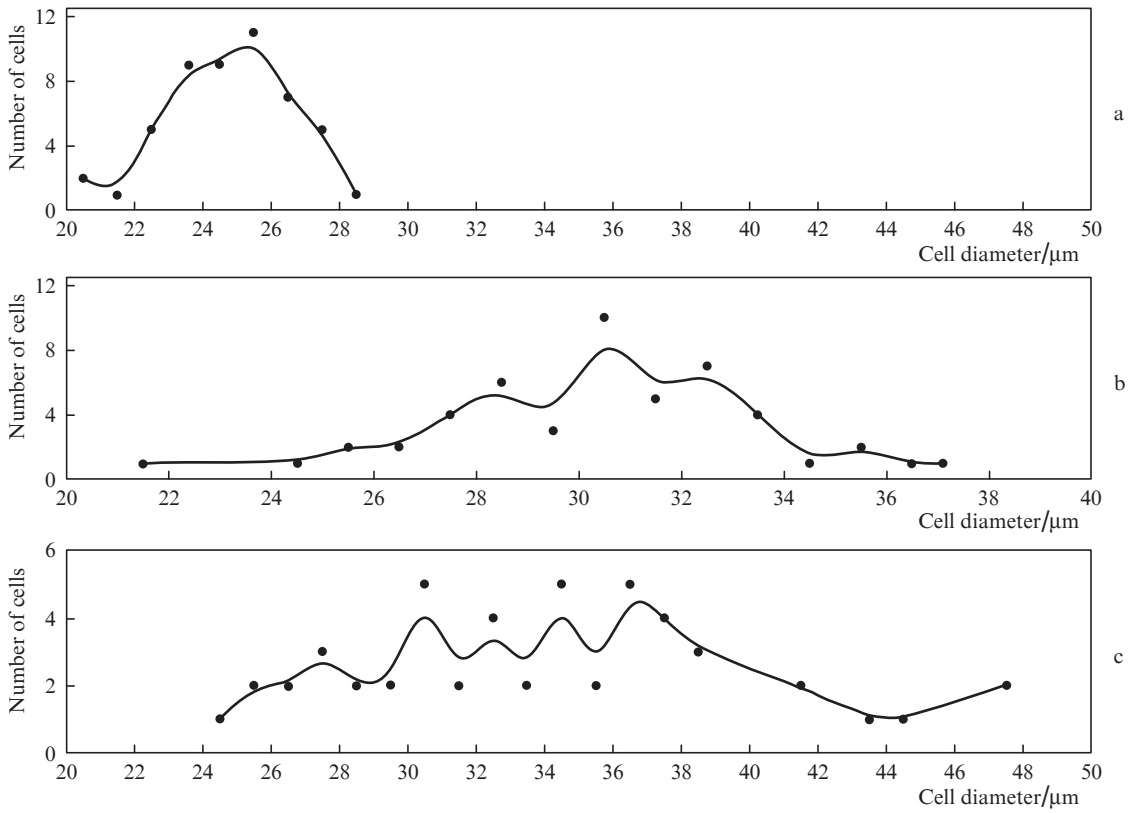

Figure 5. Cell diameter distributions for the ranges D = (a) 20–30, (b) 20–40 and (c) 20–50 μm.

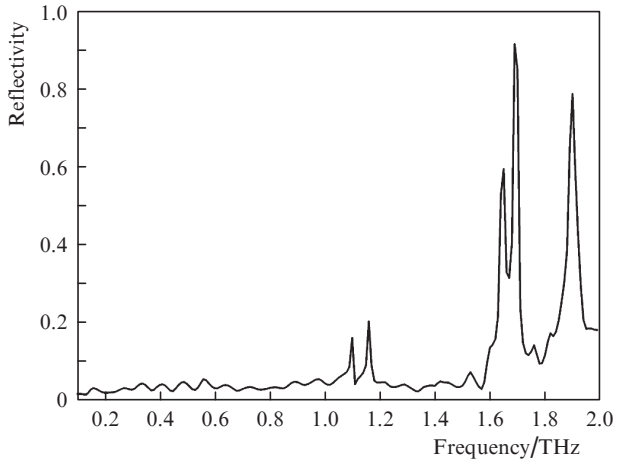

Figure 6. Measured THz reflection spectrum of the ganglion.

where $\bar{D}$ is the mean cell diameter and σ is the standard deviation. In each range, the diameters were set by a random number generator. The standard deviation in the ranges 20–30, 20–40 and 20–50 μm was 1.67, 3.34 and 3 μm, respectively. The cell diameter distribution for each range (Fig. 5) was obtained using 50 realisations.

6. Results and discussion

The measured reflection spectrum of the ganglion has weak features at frequencies of 0.34, 0.41, 0.49, 0.56, 0.64 and 0.98 THz and well-defined, strong peaks at frequencies of 1.10, 1.16, 1.65, 1.69 and 1.90 THz (Fig. 6). The spectral lines

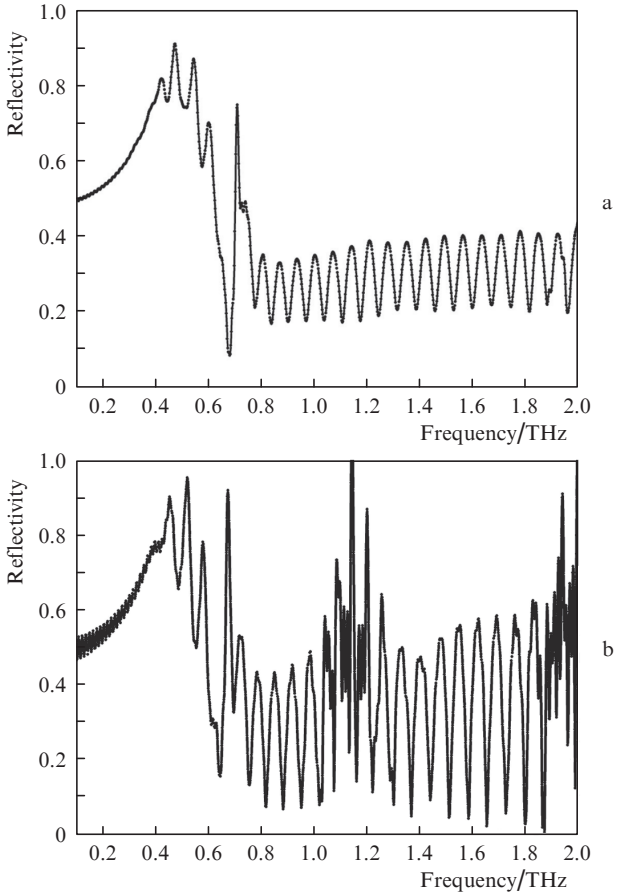

Figure 7. Simulated reflection spectra of bilayer structures: (a) substrate and object, (b) substrate and object with geometric properties of the ganglion.

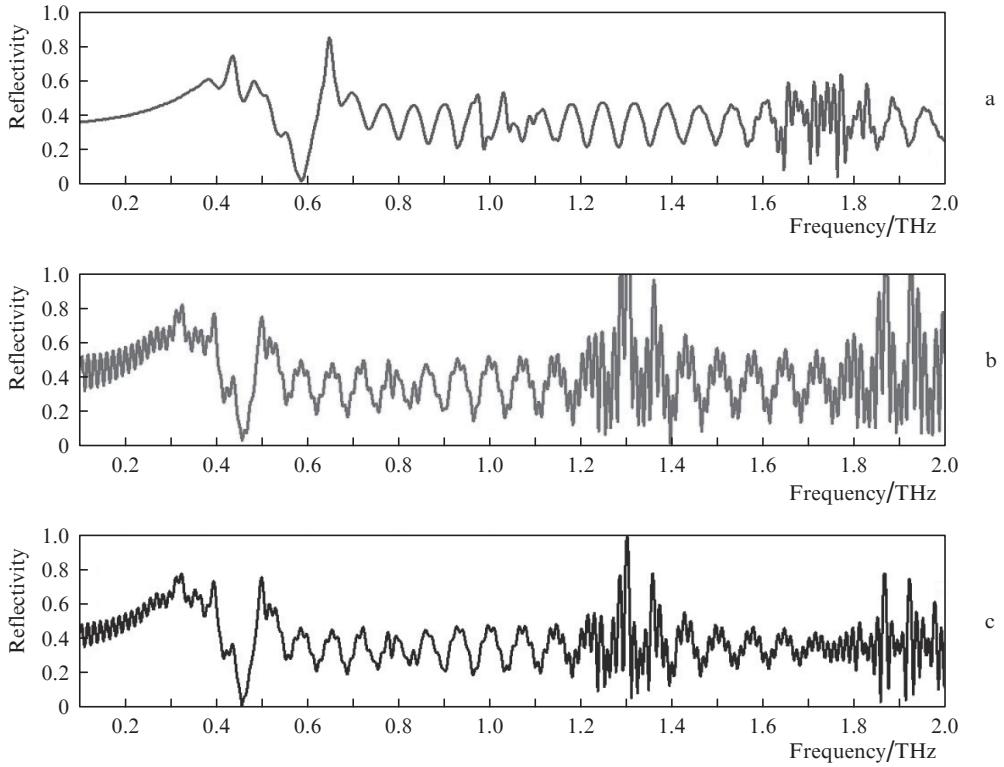

Figure 8. Simulated THz reflection spectra of nerve cells (a) 20–30, (b) 20–40 and (c) 20–50 μm in size.

at frequencies of 0.41, 0.49, 0.56 and 0.64 THz correlate well with the reflection peaks at frequencies of 0.423, 0.474, 0.544, 0.600 and 0.710 THz obtained in numerical simulation of a bilayer structure comprising a substrate and a layer of a hydrated biological object (Fig. 7a) and are due to resonance size effects over the optical length of the structure. The spectral features at frequencies above 0.80 THz obtained in numerical simulation are also due to Fabry–Perot resonances over the thickness of the structure in the case of weak dispersion of the complex permittivity of water (Fig. 3).

When the nerve cell size and spacing are taken into account, the simulated reflection spectrum contains peaks at frequencies of 1.080, 1.143, 1.200, 1.930 and 1.990 THz, which are missing in the spectrum of the structure comprising a substrate and a layer of a hydrated biological object but are present in the measured spectra (Fig. 7b). These spectral features may arise from resonance size effects of the nerve cells and are unrelated to the intermolecular interactions of hydrated cell components. To understand the origin of these features, we modelled the reflection spectra of ganglia for various nerve cell diameter distributions (Fig. 8). Varying the cell diameter distribution leads to a marked shift of the resonance peaks in the reflection spectrum, confirming the size effect on the nerve cells. The reflection spectrum in Fig. 8a contains resonances in the frequency range 1.65–1.75 THz, which correlate well with the corresponding resonances in the measured spectrum. The peaks at frequencies of 1.65 and 1.69 THz in the measured spectrum arise from resonance size effects of the cells 25 to 30 μm in diameter.

7. Analysis of results

Analysing the reflection spectra of the biological objects under study, we can identify the mechanisms underlying the effect of THz radiation at various frequencies. In particular, it follows from comparison of the spectral lines at frequencies of 1.11, 1.67 and 1.80 THz, where the reflectivity has minima, with absorption peaks of water [17–19]* that the biological effect at these frequencies is due to the absorption of the radiation by water.

The influence of irradiation at frequencies of 1.10, 1.16, 1.65 and 1.69 THz, where the system has the highest reflectivity, can be accounted for in terms of resonance size effects, and that at the frequencies corresponding to low reflectivity (in the range 1.2–1.6 THz and below 1.0 THz) is due to the strong absorption of the radiation [20].

8. Conclusions

We have studied the mechanisms underlying the effect of pulsed THz radiation on the growth of neurites of sensory ganglia using a comparative analysis of measured reflection spectra of nerve cells (in the frequency range 0.1–2.0 THz) and spectra obtained by numerical simulation wth CST Microwave Studio. The results demonstrate that

(1) the radiation is absorbed rather strongly in the frequency range from 0.1–1.0 to 1.2–1.6 THz and that

(2) there is a resonance size effect at frequencies of 1.10, 1.16, 1.65 and 1.69 THz, due to the generation of standing waves in the biological object.

Since most of the THz pulse power is concentrated in the frequency range 0.20–1.10 THz, the influence of pulsed radiation on neurites is mainly due to energy absorption. Of particular interest are the observed single resonance frequencies

* The THz frequencies of the absorption lines of water are 0.321, 0.342, 0.420, 0.489, 0.550, 0.588, 0.648, 0.675, 0.720, 0.752, 0.988, 1.097, 1.113, 1.163, 1.208, 1.229, 1.410, 1.602, 1.661, 1.669, 1.717, 1.762 and 1.795 THz.

(1.10, 1.16, 1.65 and 1.69 THz), which can be used to expose ganglia to high-power cw THz radiation in order to activate their growth.

Acknowledgements. We are grateful to V.A. Penniyainen, A.V. Kipenko, E.V. Lopatina and B.V. Krylov (Laboratory of Physiology of Excitable Membranes, Pavlov Institute of Physiology, Russian Academy of Sciences) for their assistance in the preparation of the samples and valuable suggestions.

This work was supported by the RF Ministry of Education and Science (Promotion of Leading RF Universities Programme, Subvention No. 074-U01) and OPTEC (2013 Young Scientist Contest).

References

1. Markelz A.G., Roitberg A., Heilweil E.J. *Chem. Phys. Lett.*, **320**, 42 (2000).
2. Rahman A., Stanley B., Rahman A.K. *Proc. SPIE Int. Soc. Opt. Eng.*, **7568**, 756810 (2010).
3. Walther M., Fischer B., Schall M., Helm H., Jepsen P. Uhd. *Chem. Phys. Lett.*, **332**, 389 (2000).
4. Markelz A.G., Whitmirre S., Hillebrecht J., Birge R. *Phys. Med. Biol.*, **47**, 3797 (2002).
5. Tsurkan M.V., Balbekin N.S., Sobakinskaya E.A., Panin A.N., Vaks V.L. *Opt. Spectrosc.*, **114** (6), 894 (2013).
6. Wilmink G.J., Grundt J.E. *J. Infrared, Millimeter Terahertz Waves*, **32**, 1074 (2011).
7. Frohlich H. *Proc. Natl. Acad. Sci. USA*, **72** (11), 4211 (1975).
8. Alexandrov B.S., Gelev V., Bishop A.R., Usheva A., Rasmussen K.Ø. *Phys. Lett. A*, **374** (10), 1214 (2010).
9. Chitanvis S.M. *J. Polym. Sci., Part B: Polym. Phys.*, **44** (18), 2740 (2006).
10. Munzarova A.F., Zelentsov E.L., Kozlov A.S. *Vestn. Novosibirsk. Gos. Univ., Ser. Fiz.*, **8** (2), 117 (2013).
11. Alexandrov B.S., Phipps M.L., Alexandrov L.B., Booshehri L.G., Erat A., Zabolotny J., Mielke C.H., Chen H.T., Rodriguez G., Rasmussen K.Ø., Martinez J.S., Bishop A.R., Usheva A. *Sci. Rep.*, **3**, 1184 (2013).
12. Vay S.L., Meier C., Glees P. *Acta Neuropathol.*, **17**, 103 (1971).
13. Tsurkan M.V., Penniyainen V.A., et al. *Proc. SPIE Int. Soc. Opt. Eng.*, **8261**, 82610S (2012).
14. Rønne C., Thrane L., Åstrand P.-O., Wallqvist A., Mikkelsen K.V., Keiding S.R. *J. Chem. Phys.*, **107**, 5319 (1997).
15. Rønne C., Åstrand P.-O., Keiding S.R. *Phys. Rev. Lett.*, **82** (14), 2888 (1999).
16. Naftaly M., Miles R.E. *Proc. IEEE*, **95**, 8 (2007).
17. Globus T., Bykhovski A., Khromova T., Gelmont B., Tamm L.K., Salay L.K. *Proc. SPIE Int. Soc. Opt. Eng.*, **6772**, 67720S (2007).
18. Roggenbuck A., Schmitz H., Deninger A., Cámara Mayorga I., Hemberger J., Güsten R., Grüninger M. *New J. Phys.*, **12**, 043017 (2010).
19. Exter M., Fattinger Ch., Grischkowsky D. *Opt. Lett.*, **14**, 1128 (1989).
20. Bassan P., Byrne H.J., Bonnier F., Lee J., Dumas P., Gardner P. *Analyst*, **134**, 1586 (2009).